

Core-valence double photoionization of atomic mercury

M. Huttula* and S.-M. Huttula

Department of Physics, P.O. Box 3000, 90014 University of Oulu, Oulu, Finland

S. Fritzsche

*Helmholtz-Institut Jena, Fröbelstieg 3, D-07743 Jena, Germany;**Theoretisch-Physikalisches Institut, Friedrich-Schiller-Universität Jena, Max-Wien-Platz 1, D-07743 Jena, Germany;**and Department of Physics, P.O. Box 3000, 90014 University of Oulu, Oulu, Finland*

P. Lablanquie, F. Penent, J. Palaudoux, and L. Andric

*LCPMR, UMR 7614, Université Pierre et Marie Curie - Paris 06, Sorbonne Universités, 75231 Paris Cedex 05, France**and LCPMR, UMR 7614, CNRS, 11 rue Pierre et Marie Curie, 75231 Paris Cedex 05, France*

(Received 1 October 2013; published 17 January 2014)

Multielectron coincidence spectroscopy has been used to study core $4f$ valence $5d$, $6s$ double photoionization of atomic mercury. Multiconfiguration Dirac–Fock calculations were performed to calculate the energies and to estimate the single-photon intensities of the $4f^{13}(5d^96s^2 + 5d^{10}6s^1)$ double-ionized states of atomic mercury. Reasonable agreement between the measured and simulated spectra is found if the relaxation effects of the bound-state density is taken into account in the computation of the photoionization amplitudes.

DOI: [10.1103/PhysRevA.89.013411](https://doi.org/10.1103/PhysRevA.89.013411)

PACS number(s): 32.80.Fb, 32.80.Hd

I. INTRODUCTION

Electron spectroscopy is a well-established method for studies of electronic structure in various forms of matter. Presently, third-generation synchrotron radiation sources and very-high-resolution electron spectrometers are common tools for experimentalists. To study multiple photoionization processes various multielectron coincidence setups have also been developed [1]. In our studies, the magnetic bottle multielectron coincidence apparatus developed by Eland *et al.* [2] has been implemented for use with synchrotron radiation (SR) [3] and has been applied to studies of multiple photoionization in various rare gas atoms (see, for instance, Refs. [3–5]). The very high efficiency of the magnetic bottle has also provided superior means to the experimental studies of single-photon-induced double and multiple photoionization. Such experiments have recently been performed on several gas phase atoms and molecules for core-core- [6–8] and core-valence-type of transitions [9–12].

Mercury is a liquid metal at room temperature whose electronic ground-state configuration is determined by the filled $4f$, $5d$, and $6s$ orbitals outside a xenon structure ($[Xe]4f^{14}5d^{10}6s^2$) (the $4f$ orbital being deeper than $5p$ orbitals). Even due to the recognized environmentally and human health-hazardous nature of several mercury compounds, it is still widely used, for example, in mining, the cosmetics industry, and manufacturing of fluorescent lamps. The electronic structure of mercury atoms has been investigated on solid- and vapor-phase photoionization by Svensson *et al.* [13] in the 70s using x-ray-tube radiation for ionization. The relative cross sections, branching ratios, and angular distributions of electrons has been further studied by Kobrin *et al.* [14]. The main Auger decay pathways of $4f$ core vacancy has been analyzed by Aksela *et al.* [15]. The ionized states of Hg

have been studied by several authors, mostly with optical spectroscopy [16–21], the most recent work [22] used the multielectron coincidence technique relating the previously observed optical spectra to the absolute binding-energy scale.

In the present work, we investigate the core-valence $4f^{-1}(5d^{-1}$ or $6s^{-1})$ doubly ionized states of mercury by applying multielectron coincidence spectroscopy together with synchrotron radiation excitation. To analyze the observed spectra, multiconfiguration Dirac–Fock calculations were performed to calculate the energies and to estimate the single-photon intensities of the $4f^{13}(5d^96s^2 + 5d^{10}6s^1)$ double ionization of atomic mercury. The results demonstrate the capability of the present coincidence experiment in combination with synchrotron-radiation ionization to resolve the states of direct double-electron emission previously unreachable by conventional electron spectroscopy. The comparison between the calculations and the experimental findings show the usefulness of the present approach in understanding the many-body phenomena where a detailed theoretical description is extremely difficult.

II. EXPERIMENTS

The experiments were carried out at the SOLEIL synchrotron radiation source in Saint-Aubin (France). The magnetic bottle multielectron coincidence spectrometer, described in Ref. [3] was used at the PLEIADES beamline [23–27], which covers the energy range of 7–1000 eV. Liquid Hg was evaporated to the gas phase using a resistively heated oven. Previously, because the electrons have a relatively long time of flight (up to 5 μ s), a specially designed chopper [28,29] was used to decrease the single-bunch pulse frequency of the storage ring to a 80 kHz pulse repetition rate. In the present measurements, the chopper was not used in order to maximize the count rate with the flux obtained at the beamline. The separation of the light pulses in a single-bunch mode of SOLEIL synchrotron is $T = 1184$ ns.

*marko.huttula@oulu.fi

The time of flight of slow photoelectrons can be longer than T and could be only measure modulo $[T]$. However, since in core-valence double ionization, two photoelectrons are emitted that are followed by at least one fast Auger electron that arrives within a single 1184 ns period there is no longer ambiguity on the ionizing light bunch and the absolute time of flight of the two photoelectrons are measured with respect to the good ring clock signal. The way to do is to select three-electron coincidence events with one Auger electron in the energy windows [47–57 eV] corresponding to the decay of core-valence doubly ionized states. Electron time of flights are measured by a time-to-digital converter (TDC) with a 250 ps resolution. The TDC acquisition procedure is initiated by the detection of a first electron (START), which opens a gate for 8 μ s during which the arrival times of successive electrons are measured as well as the (delayed) ring clock signal. The TOF of electrons are determined as the time difference between their arrival and this ring clock signal.

Photon-energy calibration of the monochromator was checked by measuring the total electron yield of autoionizing He doubly excited states below the $\text{He}^+(N=2)$ threshold. The TOF to kinetic-energy calibration was performed by measuring the $N=2$ photoelectron satellite line of helium at a number of kinetic energies starting from threshold. The helium $N=1$ line was used for kinetic energies above 40 eV. This calibration was cross checked with the positions of the double-ionized states of mercury, where the $5d^8 6s^2(^1S_0)$ state was taken to be at 48.90 eV binding energy [30]. Small energy shifts induced by different experimental conditions (e.g., deposition of mercury in the chamber inducing contact potentials) were corrected as constant energy shifts using a strong autoionization Auger line $5d^9_{3/2} 6p^2(^1S_0) \rightarrow 5d^{10}(^1S_0)$ at 0.55 eV of excited mercury atoms as an autocalibration point for low kinetic energy. See Ref. [22] for further details.

The detection efficiency of the magnetic bottle was deduced through the ratio of Kr $3d$ photoelectron detected (or not) in coincidence with Auger electrons and was found to be around 63% for electrons from 0 to 200 eV allowing effective detection of 25% for three electrons and 15% for four electrons in coincidence.

III. CALCULATIONS

A. Amplitudes for double photoionization

To model the simultaneous ionization of two electrons in a weak photon field, we need suitable photoionization amplitudes with two electrons in the continuum and with a change in the bound-state configurations from $5d^{10} 6s^2(^1S_0)$ ground to the $4f^{13} 5d^9 6s^2 + 4f^{13} 5d^{10} 6s$ core-valence states of mercury. Since the electron-photon interaction only acts upon a single electron at a given moment (within the weak radiation field at a synchrotron), such a double-ionization process occurs formally only in second- or higher-order perturbation theory and requires (at least) one *additional* electron-electron interaction in order to allow the emission of two electrons. Until now, however, no rigorous computational scheme has been developed that enables one to compute such second-order processes with two electrons in the continuum for correlated many-electron systems owing to the complexity of the associated continua.

In the past, *shake-up* or *shake-off* probabilities for the simultaneous excitation or ionization of some valence electron were estimated from the overlap of the one-electron orbitals, if the wave functions of the initial and final bound-states were calculated separately. This model assumes that the major part of the excess energy is given to the photoionization of one (the core) electron, while a second (weakly bound valence) electron is released into the continuum owing to the rapid change in the atomic potential. Only very recently [11,31], we have developed a computational approach in which the two-electron continua are taken into account explicitly. Here, we shall give a brief account on the computational procedure but otherwise refer the reader for further details to the reference above.

Within the electric-dipole approximation, the double photoionization of atoms and ions is formally described by means of the (dipole) amplitudes

$$D(\omega; \gamma_f J_f P_f, \epsilon_1 \kappa_1, \epsilon_2 \kappa_2 : \gamma_i J_i P_i), \quad (1)$$

which connects the initial state $|\psi_i\rangle \equiv |\psi(\gamma_i J_i P_i)\rangle$ of the atom to the final state $|\psi(\gamma_f J_f P_f)\rangle$ of the photoion, and with two photoelectrons in the continuum. In this notation of the double photoionization process, it is assumed that the photoelectrons escape as two partial waves $|\epsilon_1 \kappa_1\rangle$ and $|\epsilon_2 \kappa_2\rangle$ with angular momentum (quantum numbers; $i = 1, 2$) $\kappa_i = \pm(j + 1/2)$ for $l = j \pm 1/2$, and with the kinetic energies ϵ_1 and ϵ_2 , respectively. Only the sum of these two energies $\epsilon_1 + \epsilon_2 = E_i + \omega - E_f$ is determined owing to the conservation of energy by the total energy of the system as defined on the right-hand side of the expression. However, rather a large or even huge number of total final states $|\psi_t\rangle = |\gamma_f J_f P_f, \epsilon_1 \kappa_1, \epsilon_2 \kappa_2, : \gamma_i J_i P_i\rangle$ occurs for the overall system “photoion + two electrons,” and all with total energy $E_t \equiv E_f + \epsilon_1 + \epsilon_2 = E_i + \omega$. They arise from the different coupling possibilities of the two outgoing electrons to the (total) angular momentum of the photoion, so that $|J_i - 1| \leq J_t \leq |J_i + 1|$ and $P_t = \bar{P}_i$ is fulfilled within the electric-dipole approximation, and which makes an accurate computation of these amplitudes a real challenge even for present-day computers [32].

From the amplitudes (1), the cross section (intensity) for the simultaneous emission of two electrons,

$$\sigma = \frac{4\pi^2 \alpha \omega}{3(2J_i + 1)} \sum_{\kappa_1, \kappa_2, J_t} \int d\epsilon_1 \times |D(\omega; \gamma_f J_f P_f, \epsilon_1 \kappa_1, \epsilon_2 \kappa_2 : \gamma_i J_i P_i)|^2, \quad (2)$$

is obtained by a summation over the partial waves κ_1, κ_2 of the emitted electrons and the total angular momentum of J_t of the overall scattering states as well as by an integration over one of the free electrons. The energy of the second electron, ϵ_2 , is then determined by energy conservation. Moreover, since the initial states has $J_i = 0$, the summation over the total angular momentum is restricted to $J_t = 1$ in the present case (and the electric-dipole approximations). In practice, however, computation of these dipole amplitudes is hampered by the fact that the initial and final ionic (bound) states have a quite different electronic structure, i.e., occupation of the electronic shells. This difference gives a zero amplitude if calculated with a frozen set of atomic orbitals and remains tiny if typical electronic correlations are taken into account.

To avoid the (unfeasible) summation over the complete many-electron continuum in second-order perturbation theory, a rather rough but justified approximation is based on the relaxation of the electron density over the course of the photoionization process together with the computation of such “relaxed-orbital” amplitudes [33,34]. The separate optimization of the bound states, namely, leads to (two sets of) electron orbitals which are not quite orthogonal to each other and which are able to capture a significant part of the correlations among the electrons. In this approximation, then, a nonzero amplitude arises for various single-photon processes already with the standard definition of the photoionization amplitudes if the overlap of all the one-electron orbitals is taken properly into account. It is this approach that has been utilized in the present work [35].

B. Wave functions and intensities for double ionization

As outlined above, the single-photon double ionization of atoms and ions cannot be understood without a proper treatment of the *correlated* wave functions. To generate these wave functions for the initial and final ionic states, the multiconfiguration Dirac–Fock (MCDHF) method [35,36] has been utilized and combined with partial waves for the outgoing electrons. In particular, the GRASP92 code [37] has been utilized to compute the $5d^{10}6s^2\ ^1S_0$ ground and the $4f^{-1}5d^96s^2 + 4f^{-1}5d^{10}6s$ core-valence states of mercury. Apart from the Dirac–Coulomb Hamiltonian, moreover, the Breit interaction was added to the representation of the bound-state density but not to the orbital functions themselves.

To estimate the relative intensities for the double ionization of atomic mercury, the PHOTO component of the RATIP program [38,39] has been adapted to deal with two electrons in the continuum. To this end, two partial waves with proper energy sharing are coupled to the states of the photoion in order to generate scattering states with proper energy and symmetry within the continuum. All continuum spinors are solved within a spherical but level-dependent potential of the final ion (the so-called *optimal-level* scheme within the GRASP92 program) and by including the exchange interaction of the emitted electron with the bound-state density. For further details on the computations of the photoionization amplitudes, we refer the reader to Refs. [31,35]. However, little is known so far of how this approximation works for calculating the (double-differential) photoionization cross sections with different energy sharing among the two electrons. Despite the rather crude model for calculating these intensities for different final states of the photoion, the comparison below shows overall a very reasonable agreement between theory and experiment. It is therefore interesting to further analyze this model for other photon energies as well as explicitly for different relative energies of the (two) emitted electrons.

IV. RESULTS AND DISCUSSION

A. Double photoionization

The population of the $4f^{-1}V^{-1}$ double photoionization final states was obtained from the multielectron coincidence data-set collected at the photon energy of 175.8 eV. To separate the two simultaneously emitted core-valence electrons from

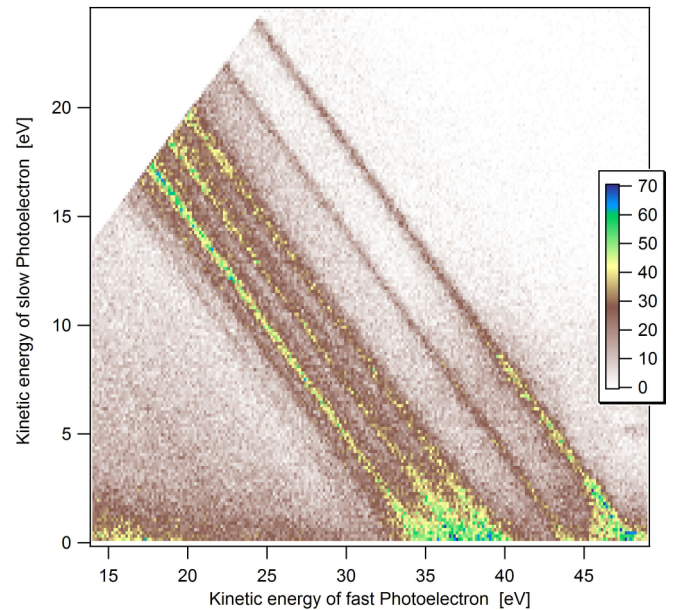


FIG. 1. (Color online) Energy correlation between the two photoelectrons emitted upon core-valence double photoionization. They have been detected in coincidence with a third Auger electron of 47–57 eV kinetic energy.

any other electron pairs emerging from the consecutive decay processes of either $4f$ or $5p$ ionization, a three-electron coincidence method was employed. It has been established [15] that $4f$ holes of a Hg^+4f^{-1} core-state decay mainly by emitting an Auger electron in the 59–70 eV kinetic-energy range. We observed that, for the $4f$ holes of a $\text{Hg}^{2+}4f^{-1}V^{-1}$ core-valence state, the decay proceeds by emission of an Auger electron of slightly lower kinetic energy, in the 47–57 eV kinetic-energy range. As explained in the experimental paragraph, the method consists then of filtering (core + valence) photoelectron pairs from the dataset when they have been detected in coincidence with a third (Auger) electron in the 47–57 eV kinetic-energy range. Figure 1 displays the energy correlation between the two photoelectrons, detected in coincidence with such an Auger electron. The diagonal lines correspond to the different core-valence Hg^{2+} states and display the energy sharing between the two photoelectrons. It is observed that some states present a rather uniform distribution associated with a direct double-photoionization path, while for others it is structured, indicating the presence of indirect double-photoionization paths. The experimental population of the double-photoionized states is obtained by integration of Fig. 1 along the diagonal lines and is shown in Fig. 2(a) above the theoretically simulated spectrum. In order to evaluate the experimental intensities of the observed features, the experiment was least-square fit using Voigt functions.

The first part of the spectrum with binding energies between 125 and 135 eV consists of two sharp peaks and is followed between 135 and 145 eV by a second region with seven resolvable peaks. The experimental energies and intensities are given in Table I. The small asymmetry observed on the first and second peak is seemingly an artefact arising from

TABLE I. Experimental and calculated binding energies and identification of the Hg $4f^{-1}V^{-1}$ double ionized states.

Peak	Experiment			Theory			
	Eb [eV](± 0.1)	Diff. [eV]	Intensity	Eb [eV]	Diff.	Intensity	Identification
1	127.4	0.000	146	{ 123.523 123.586	{ 0 0.063	43	$4f_{7/2}^{-1}6s^{-1}(J = 4)$ $4f_{7/2}^{-1}6s^{-1}(J = 3)$
2		4.0	77		{ 3.984 4.030	257	$4f_{5/2}^{-1}6s^{-1}(J = 2)$ $4f_{5/2}^{-1}6s^{-1}(J = 3)$
3		8.6	202		{ 7.866 8.353 8.528 8.757 8.804	165	$4f_{7/2}^{-1}5d_{5/2}^{-1}6s^2(J = 4)$ $4f_{7/2}^{-1}5d_{5/2}^{-1}6s^2(J = 5)$ $4f_{7/2}^{-1}5d_{5/2}^{-1}6s^2(J = 6)$ $4f_{7/2}^{-1}5d_{5/2}^{-1}6s^2(J = 2)$ $4f_{7/2}^{-1}5d_{5/2}^{-1}6s^2(J = 3)$
4		10.1	101		{ 10.010 10.135 10.481	67	$4f_{7/2}^{-1}5d_{3/2}^{-1}6s^2(J = 4)$ $4f_{7/2}^{-1}5d_{3/2}^{-1}6s^2(J = 3)$ $4f_{7/2}^{-1}5d_{5/2}^{-1}6s^2(J = 1)$
5		11.0	128		{ 11.075 11.543	68	$4f_{7/2}^{-1}5d_{3/2}^{-1}6s^2(J = 5)$ $4f_{7/2}^{-1}5d_{3/2}^{-1}6s^2(J = 2)$
6		12.4	92		{ 12.030 12.331 12.645	140	$4f_{5/2}^{-1}5d_{5/2}^{-1}6s^2(J = 4)$ $4f_{5/2}^{-1}5d_{5/2}^{-1}6s^2(J = 3)$ $4f_{5/2}^{-1}5d_{5/2}^{-1}6s^2(J = 2)$
7		13.4	157		{ 13.359 13.416 13.819	90	$4f_{5/2}^{-1}5d_{5/2}^{-1}6s^2(J = 1)$ $4f_{5/2}^{-1}5d_{5/2}^{-1}6s^2(J = 5)$ $4f_{5/2}^{-1}5d_{5/2}^{-1}6s^2(J = 0)$
8		14.5	74		{ 14.481 14.484 14.490	150	$4f_{5/2}^{-1}5d_{3/2}^{-1}6s^2(J = 3)$ $4f_{5/2}^{-1}5d_{3/2}^{-1}6s^2(J = 4)$ $4f_{5/2}^{-1}5d_{3/2}^{-1}6s^2(J = 2)$
9		16.1	21		16.151	20	$4f_{5/2}^{-1}5d_{3/2}^{-1}6s^2(J = 1)$

the overlap of decay of $5p$ photoionization satellite lines. Similarly, there may exist some nonlinearity in the background of the high-binding-energy part of the spectrum.

The simulated spectrum in Fig. 2(b) is formed convoluting the *ab-initio* transition energies and intensities with a width of 0.3 eV Gaussian and Lorentzian contributions in order to match to the experimental conditions. A remarkably good agreement between the simulated and observed spectra is found as seen this figure. According to the calculations, the two peaks at 127.4 and 131.4 eV are to the double ionization of atomic mercury to the $4f^{-1}6s^{-1}$ final states of the photoion. The splitting of the first two lines is due to the spin-orbit splitting of the $4f$. Moreover, the calculations predict two very-close-lying states at binding energies 123.52 and 123.58 eV, which are not resolved in the experiment. These close-lying states arise due to the coupling of the single valence electron to the $4f$ core hole state. The binding energy of the first line in the experiment is 127.4 eV. The prediction (123.5 eV) deviates from this by around 4 eV, being well in the expected range for such a multielectron atom. The experimental energy difference between two $4f^{-1}6s^{-1}$ states is 4.00 eV, which is well predicted by our calculations.

The second group of peaks at the binding-energy region of 135 to 145 eV consists of several transitions to $4f^{-1}5d^{-1}$ states. The calculation for this region suggest 20 contributing

transitions. While a unique identification remains a challenge for all the levels involved, the experimentally observed peaks may be traced to groups of transitions based on the high-accuracy match of the predicted distribution of binding energies (see Table I) This is also seen by the fact that the predicted spectrum in Fig. 2 reproduces the observed structures when convoluted with linewidth matching to the experiment. The energies and intensities of the final states contributing to the assigned experimental peaks are given in Table I. Comparing the predicted relative energies to the experiment it is obvious that the state distributions are predicted with the accuracy of a tenth of an eV, thus a reliable identification may be given.

As seen in Table I, rather large discrepancies between the calculated and observed (relative) populations occur due to the approximation as applied in the computations. In particular, the relative intensities of peaks 2, 6, and 8 are clearly overestimated and poorly reproduce the observed peaks. The other peaks are reproduced better. This different behavior in predicting relative intensities is not yet understood and will require further computations for different photon energies and energy sharing between the two electrons. Especially, the effects of the energy sharing need to be explored in further detail since, in contrast to our expectation, only a very small effect was found in the present model. Apart from the

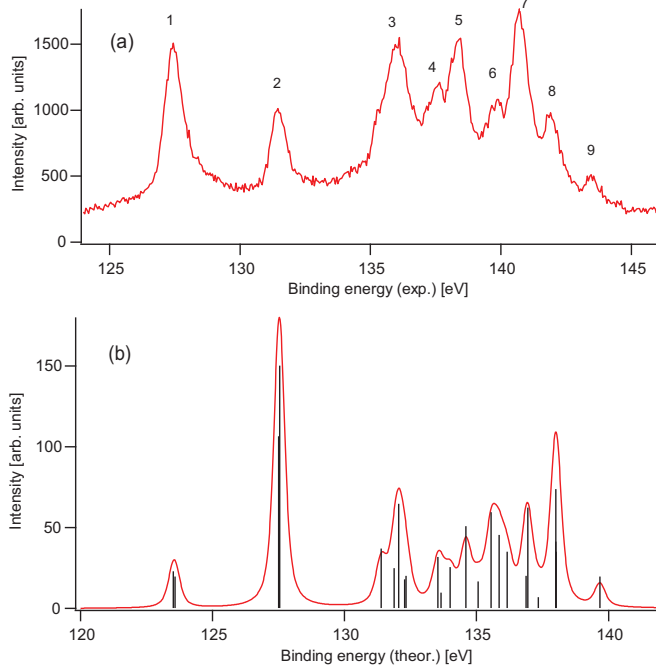


FIG. 2. (Color online) The (a) experimental and (b) predicted spectrum of the population of the $4f^{-1}V^{-1}$ double-ionized states.

relaxation model itself, such an energy dependence may arise also from the choice of the wave-function expansion.

B. Relative cross section

The relative single-to-double-ionization cross section may be experimentally determined in the magnetic-bottle experiment as the efficiency of the electron detection and is known ($63 \pm 4\%$ in the present experiment). The total number of core-valence events (the coincidences of two photo and one Auger electron) was divided by the number of detected $4f$ photoelectrons. The detection efficiency corrected observed ratios for the core-valence double to single photoionization probabilities are $3.5 \pm 1\%$, $8.2 \pm 2\%$, $7.4 \pm 2\%$, and $7.4 \pm 2\%$ for the photon energies of 150.7, 175.8, 185.9, and 200.9 eV, respectively. Note that the ratios at the two higher photon energies are expected to be underestimated because, at these photon energies, the energy range of the core-valence photoelectrons and of the Auger electrons overlap, and it is not possible to disentangle them completely. The present theoretical approach is unable to provide a prediction for the ratios as the single- and double-ionization states are optimized independently. For an accurate determination of these intensity ratios, moreover, the

transition probabilities for the various shake-up process would be needed. In comparison to our previous experiment with the aluminum $2p^{-1}V^{-1}$ direct double ionization in Ref. [40], the trend of the observed probability as a function of excess energy is similar. The maximum of the probability in Al is reached around five electron volts above the double-ionization energy. At present, the possible final states in Hg range to almost the 20 eV region, suggesting a more shallow slope for the cross section. The first photon energy selected is just around 5 eV above the last $4f^{-1}5d^{-1}$ states, providing roughly half of the maximum probability observed at 20 eV excess energy. Tentatively, the difference of the energies could be explained by the valence orbitals involved. According to Yeh and Lindau [41] the aluminum $2p$ reaches the maximum cross section in around 20 eV above the threshold, while the Hg $4f$ cross-section slope is more broad and rises up to 200 eV above the threshold. By this crude comparison it is obvious that the involvement of a valence orbital suppresses the energy scale of the cross section of double vs the corresponding single photoionization.

V. CONCLUSION

In the present work, the $4f^{-1}V^{-1}$ core and valence doubly ionized states of mercury have been observed with the aid of synchrotron radiation combined with a multielectron coincidence experiment. The relative strength of the double (core valence) to single photoionization has also been experimentally observed as a function of photon energy and shortly discussed. Relativistic Dirac-Fock calculations have been applied to identify the observed peaks in the double-ionization spectra. A reasonable agreement between experiment and theory has enabled us to assign the observed levels of the photoion. Further theoretical work is, however, needed for different photon energies and energy sharing between the two electrons to better understand the limitations of the model. The applied model for the final-state populations reasonably reproduce the trends of the experiment, thus suggesting its further usability in approximations of the double-ionization intensities.

ACKNOWLEDGMENTS

This work has been financially supported by the Research Council for Natural Sciences and engineering of the Academy of Finland. Noora Kulmala is acknowledged for the preliminary work on the calculations. The experiment was performed at SOLEIL Synchrotron (France) at the PLEIADES beam line, with the approval of the Soleil Peer Review Committee (Project No. 20100938). We are grateful to Xiaojing Liu and PLEIADES team for help during the measurements and to SOLEIL staff for stable operation of the storage ring.

- [1] L. Avaldi and A. Huetz, *J. Phys. B: At., Mol. Opt. Phys.* **38**, S861 (2005), and references therein.
 [2] J. H. D. Eland, O. Vieuxmaire, T. Kinugawa, P. Lablanquie, R. I. Hall, and F. Penent, *Phys. Rev. Lett.* **90**, 053003 (2003).
 [3] F. Penent, J. Palaudoux, P. Lablanquie, L. Andric, R. Feifel, and J. H. D. Eland, *Phys. Rev. Lett.* **95**, 083002 (2005).

- [4] P. Lablanquie, L. Andric, J. Palaudoux, U. Becker, M. Braune, J. Viehhaus, J. H. D. Eland, and F. Penent, *J. Electron Spectrosc. Relat. Phenom.* **156**, 51 (2007).
 [5] J. Palaudoux, P. Lablanquie, L. Andric, K. Ito, E. Shigemasa, J. H. D. Eland, V. Jonauskas, S. Kucas, R. Karazija, and F. Penent, *Phys. Rev. A* **82**, 043419 (2010).

- [6] P. Lablanquie, F. Penent, J. Palaudoux, L. Andric, P. Selles, S. Carniato, K. Bucar, M. Zitnik, M. Huttula, J. H. D. Eland, E. Shigemasa, K. Soejima, Y. Hikosaka, I. H. Suzuki, M. Nakano, and K. Ito, *Phys. Rev. Lett.* **106**, 063003 (2011).
- [7] J. H. D. Eland, M. Tashiro, P. Linusson, M. Ehara, K. Ueda, and R. Feifel, *Phys. Rev. Lett.* **105**, 213005 (2010).
- [8] M. Nakano, F. Penent, M. Tashiro, T. P. Grozdanov, M. Zitnik, S. Carniato, P. Selles, L. Andric, P. Lablanquie, J. Palaudoux, E. Shigemasa, H. Iwayama, Y. Hikosaka, K. Soejima, I. H. Suzuki, N. Kouchi, and K. Ito, *Phys. Rev. Lett.* **110**, 163001 (2013).
- [9] J. Niskanen, V. Carravetta, O. Vahtras, H. Ågren, H. Aksela, E. Andersson, L. Hedin, P. Linusson, J. H. D. Eland, L. Karlsson, J.-E. Rubensson, and R. Feifel, *Phys. Rev. A* **82**, 043436 (2010).
- [10] E. Andersson, J. Niskanen, L. Hedin, J. H. D. Eland, P. Linusson, L. Karlsson, J.-E. Rubensson, V. Carravetta, H. Ågren, and R. Feifel, *J. Chem. Phys.* **133**, 094305 (2010).
- [11] E. Andersson, P. Linusson, S. Fritzsche, L. Hedin, J. H. D. Eland, L. Karlsson, J. E. Rubensson, and R. Feifel, *Phys. Rev. A* **85**, 032502 (2012).
- [12] S. M. Huttula, P. Lablanquie, L. Andric, J. Palaudoux, M. Huttula, S. Sheinerman, E. Shigemasa, Y. Hikosaka, K. Ito, and F. Penent, *Phys. Rev. Lett.* **110**, 113002 (2013).
- [13] S. Svensson, N. Mårtensson, E. Basilier, P. Å. Malmquist, U. Gelius, and K. Siegbahn, *J. Electron Spectrosc. Relat. Phenom.* **9**, 51 (1976).
- [14] P. H. Kobrin, P. A. Heimann, H. G. Kerckhoff, D. W. Lindle, C. M. Truesdale, T. A. Ferrett, U. Becker, and D. A. Shirley, *Phys. Rev. A* **27**, 3031 (1983).
- [15] H. Aksela, S. Aksela, J. S. Jen, and T. D. Thomas, *Phys. Rev. A* **15**, 985 (1977).
- [16] R. B. Cairns, H. Harrison, and R. I. Schoen, *J. Chem. Phys.* **53**, 96 (1970).
- [17] J. H. D. Eland and R. Feifel, *J. Phys. Chem. A* **108**, 9721 (2004).
- [18] Y. N. Joshi, A. J. J. Raassen, and B. Arcimowicz, *J. Opt. Soc. Am. B* **6**, 534 (1989).
- [19] A. A. van der Valk, A. A. Raassen, and Y. N. Joshi, *J. Opt. Soc. Am. B* **7**, 1182 (1990).
- [20] A. J. J. Raassen, Y. N. Joshi, and A. Tauheed, *Phys. Scr.* **43**, 44 (1991).
- [21] J.-F. Wyart, A. J. J. Raassen, G. J. van het Hof, and Y. N. Joshi, *Phys. Scr.* **47**, 784 (1993).
- [22] M. Huttula, S.-M. Huttula, P. Lablanquie, J. Palaudoux, L. Andric, J. H. D. Eland, and F. Penent, *Phys. Rev. A* **83**, 032510 (2011).
- [23] C. Miron *et al.*, <http://www.synchrotron-soleil.fr/Recherche/LignesLumiere/PLEIADES>.
- [24] O. Travnikova, J. C. Liu, A. Lindblad, C. Nicolas, J. Söderström, V. Kimberg, F. Gel'mukhanov, and C. Miron, *Phys. Rev. Lett.* **105**, 233001 (2010).
- [25] J. Stöderström, A. Lindblad, A. Grum-Grzhimailo, O. Travnikova, C. Nicolas, S. Svensson, and C. Miron, *New J. Phys.* **13**, 073014 (2011).
- [26] C. Miron, C. Nicolas, O. Travnikova, P. Morin, Y. P. Sun, F. Gel'mukhanov, N. Kosugi, and V. Kimberg, *Nat. Phys.* **8**, 135 (2012).
- [27] A. Lindblad, V. Kimberg, J. Söderström, C. Nicolas, O. Travnikova, N. Kosugi, F. Gel'mukhanov, and C. Miron, *New J. Phys.* **14**, 113018 (2012).
- [28] Y. Hikosaka, P. Lablanquie, F. Penent, T. Kaneyasu, E. Shigemasa, R. Feifel, J. H. D. Eland, and K. Ito, *Phys. Rev. Lett.* **102**, 013002 (2009).
- [29] K. Ito, F. Penent, Y. Hikosaka, E. Shigemasa, I. H. Suzuki, J. H. D. Eland, and P. Lablanquie, *Rev. Sci. Instrum.* **80**, 123101 (2009).
- [30] C. E. Moore, *Atomic Energy Levels, US National Bureau of Standards* (US Government Printing Office, Washington DC, 1971), Vol. 1.
- [31] P. Linusson, S. Fritzsche, J. H. D. Eland, M. Mucke, and R. Feifel, *Phys. Rev. A* **87**, 043409 (2013).
- [32] N. M. Kabachnik, S. Fritzsche, A. G. Grum-Grzhimailo, M. Meyer, and K. Ueda, *Phys. Rep.* **451**, 155 (2007).
- [33] S. Fritzsche, B. Fricke, and W.-D. Sepp, *Phys. Rev. A* **45**, 1465 (1992); S. Fritzsche, *ibid.* **180**, 262 (1993).
- [34] S. Fritzsche, *J. Electron Spectrosc. Relat. Phenom.* **114**, 1155 (2001).
- [35] S. Fritzsche, *Phys. Scr. T* **100**, 37 (2002).
- [36] I. P. Grant, in *Methods in Computational Chemistry*, edited by S. Wilson (Plenum Press, New York, 1988), Vol. 2, p. 1.
- [37] F. A. Parpia, C. F. Fisher, and I. P. Grant, *Comput. Phys. Commun.* **94**, 249 (1996).
- [38] S. Fritzsche, *Comput. Phys. Commun.* **183**, 1525 (2012).
- [39] S. Fritzsche, J. Nikkinen, S.-M. Huttula, H. Aksela, M. Huttula, and S. Aksela, *Phys. Rev. A* **75**, 012501 (2007).
- [40] K. Jänkälä, S. Fritzsche, M. Huttula, J. Schulz, S. Urpelainen, S. Heinäsmäki, S. Aksela, and H. Aksela, *J. Phys. B* **40**, 3435 (2007).
- [41] J. J. Yeh and I. Lindau, *At. Data Nucl. Data Tables* **32**, 1 (1985).